The Canadian Mineralogist
Vol. 54, pp. 1249-1259 (2016)
DOI: 10.3749/canmin.1400101

MEIERITE, A NEW BARIUM MINERAL WITH A KFI-TYPE ZEOLITE FRAMEWORK FROM THE GUN CLAIM, YUKON CANADA

R.C. PETERSON[§]

Department of Geological Sciences and Geological Engineering, Queen's University, Kingston, Ontario, Canada, K7L 3N6

GUNNAR FARBER

Bornsche Str. 9,39326 Samswegen, Germany

R. JAMES EVANS AND LEE GROAT

Department of Earth, Ocean and Atmospheric Sciences, University of British Columbia Vancouver, British Columbia, Canada V6T 1Z4

LAURA MACNEIL AND BRIAN JOY

Department of Geological Sciences and Geological Engineering, Queen's University, Kingston, Ontario, Canada, K7L 3N6

BARBARA LAFUENTE

PANalytical, 7602 EA Almelo, Netherlands

THOMAS WITZKE

Department of Geosciences, University of Arizona, Arizona, USA

ABSTRACT

Meierite, ideally $Ba_{44}Si_{66}Al_{30}O_{192}Cl_{25}(OH)_{33}$, is a new mineral from the Gun claim, just south of the Itsi Range, Yukon, Canada. Meierite occurs as equant grains up to 200 μm across, enclosed within large gillespite crystals. The mineral is transparent, has a vitreous luster, and is non-fluorescent. It has a white streak and Mohs hardness of approximately 5½. It is brittle with no observed cleavage. The calculated density based upon the chemical formula and single-crystal unit-cell dimension is 3.50 g/cm^3. The mineral is optically isotropic ($n = 1.598$) Electron-microprobe composition (average of 11): SiO_2 28.30, P_2O_5 1.61, Al_2O_3 11.75, TiO_2 0.05, FeO 0.27, CaO 0.21, BaO 47.61, Na_2O 0.15, K_2O 0.21, Cl 6.64, and a total of 95.29 wt.%. The empirical formula (based on 192 framework O *apfu*) and charge balance considerations is: $Ba_{41.1}Ca_{0.5}Fe_{0.5}Na_{0.7}K_{0.6}Si_{62.5}Al_{30.5}P_{3.0}O_{192}Cl_{24.8}\cdot 33.4(OH)$. It is possible that additional H_2O molecules are located within the cavities in the structure. Meierite is cubic, $Im\bar{3}m$, a 18.5502(4) Å, V 6383.3(2) Å^3, and $Z = 1$. The 10 most intense lines in the X-ray powder diffraction pattern are [d_{obs} in Å(I)(hkl)]: 4.39(70)(411), 4.16(26)(420), 3.798(25)(422), 3.288(34)(440), 3.189(100)(433), 3.016(72)(611), 2.803(42)(622), 2.629(31)(710), 2.323(46)(800), and 2.287(59)(741).

The crystal structure ($R = 4.1\%$ for 1393 $F_o > 4\sigma F$) is a three dimensional framework of silicon-, aluminium-, and phosphorous-containing tetrahedra that create an open framework consisting of a large cubo-octahedral cavity connected by channels composed of double eight-membered rings and double six-membered rings. The aluminosilicate framework is isostructural with that observed for silicate framework type ZK-5 (KFI). The mineral is named in honor of Walter M. Meier (1926–2009), a pioneer in zeolite research.

Keywords: zeolite, crystal structure, new mineral, Gun Claim, Yukon, Canada.

§ *Corresponding author e-mail address*: peterson@queensu.ca

Introduction

The Gun Claim is located approximately 5 km southeast of the Itsi Lakes and approximately 363 km northeast of Whitehorse, Yukon, Canada. The longitude and latitude coordinates of the claim are 130°0′51″W, 62°50′50″N (Fig. 1). The nearest road is the Canol Road, located 26 km northwest of the claim; this road is only useable in the summer months. The nearest town is Ross River, located approximately 162 km southwest of the claim. The Gun Claim itself is accessible only by helicopter.

The Gun Claim area was first explored by Joseph Keele, who explored the upper Pelly and Ross Rivers in 1907 and 1908, but no further exploration was completed until 1944, when E.D. Kindle conducted geological field work along the Canol Road (Montgomery 1960). A sample containing gillespite ($BaFeSi_4O_{10}$) was submitted by Scotty Alan of Newmont Mining Corporation to Dr. R.M. Thompson of the University of British Columbia in 1957, which became the catalyst for an investigation of the area in 1958 termed "Operation Pelly" by the Geological Survey of Canada. Specimens collected during the field season in 1958 were later analyzed at the University of British Columbia in 1959 and 1960 by Joseph Hilton Montgomery (Montgomery 1960). Montgomery's work included the discovery of a new calcium-iron-aluminosilicate mineral which he named keeleite, but this name was later changed to pellyite [$Ba_2Ca(Fe^{2+},Mg)_2Si_6O_{17}$] in 1972 after further investigation (Montgomery *et al*. 1972). Along with this discovery, Montgomery was able to identify several other barium silicate minerals, such as taramellite [$Ba_4(Fe^{3+},Ti,Fe^{2+},Mg)_4(B_2Si_8O_{27})O_2Cl_x$], gillespite ($BaFe^{2+}Si_4O_{10}$), and sanbornite ($Ba_2Si_4O_{10}$), all of which had been described from a locality in California prior to 1960 (Montgomery 1960). The Gun Claim is also a locality for the minerals titantaramellite (Alfors & Pabst 1984) and itsiite (Kampf *et al*. 2014).

Similar deposits were discovered in 1932 at Trumbull Peak, Mariposa County, California, where the mineral sanbornite was first discovered and was found associated with gillespite, taramellite, and celsian. After this discovery at Trumbull Peak, several other occurrences of sanbornite and gillespite were found at Big Creek, Fresno County in 1957 by G.M. Landers and Rush Creek in 1960 by R.E. Walstrom (Alfors *et al*. 1965). The discovery of these occurrences resulted in a field study in 1961 by the California Division of Mines and Geology to determine the geologic setting and the potential commercial value of the deposits of eastern Fresno County (Alfors *et al*. 1965). This study resulted in the identification of several new barium silicate minerals including macdonaldite $BaCa_4Si_{16}O_{36}(OH)_2{\cdot}10H_2O$, krauskopfite $BaSi_2O_4(OH)_2{\cdot}2H_2O$, walstromite $BaCa_2Si_3O_9$, fresnoite $Ba_2TiOSi_2O_7$, verplanckite $Ba_2(Mn,Fe,Ti)Si_2O_6(OH,O,Cl,F)_2{\cdot}3H_2O$, muirite $Ba_{10}Ca_2Mn^{2+}TiSi_{10}O_{30}(OH,Cl,F)_{10}$, and traskite $Ba_9Fe_2^{2+}Ti_2(SiO_3)_{12}(OH,Cl,F)_6{\cdot}6H_2O$, along with alforsite $Ba_5(PO_4)_3Cl$, a barium apatite, which was later described from Big Creek (Alfors *et al*. 1965, Newberry *et al*. 1981). In addition, cerchiaraite-(Fe) $Ba_4Fe^{3+}{}_4O_3(OH)_3(Si_4O_{12})[Si_2O_3(OH)_4]Cl$ and cerchiaraite-(Al) were described in Kampf *et al*. (2013). The California deposits are referred to as the "Sanbornite Deposits," as most of the barium minerals discovered at these localities are present within quartz-sanbornite outcrops (Walstrom & Leising 2005).

Fig. 1. The Gun Claim looking north. Small trenches can be seen near the end of the small unnamed lake.

Geological Setting

This area surrounding the Gun Claim consists of several intrusive stocks ranging in composition from quartz monzonite to granodiorite that are Cretaceous in age and are the result of accretion during the Cordilleran Orogeny (Montgomery 1960). Two skarn deposits have been found associated with a quartz monzonite stock that has an area of approximately 13 km^2 (Montgomery 1960). The first skarn, known as the Birr Claim, is located 2 km southeast of the Gun Claim. The Birr Claim hosts a Cu skarn consisting of pyrrhotite, chalcopyrite, and gillespite developed in Ordovician–Devonian sedimentary rocks at the margin of the quartz monzonite stock. Barite veins have also been found near the intrusive contact (Yukon Geological Survey Minfile # 105I 007, 1992). The second skarn (Pb-Zn) is on the Gun Claim (Fig. 1). Here, mineralized zones are the result of hydrothermal alteration by fluids originating from the

quartz monzonite stock. These fluids resulted in hornfels metamorphism and the creation of skarns in the adjacent sedimentary package, which consists of argillite, limestone, shale, slate, and quartzite (Yukon Geological Survey Minfile #105J 015, 1992). Mineralized zones consist of sphalerite and chalcopyrite, which occur with pyrrhotite, barite, witherite, and several rare barium silicate minerals (Montgomery 1960). These zones occur in pyroxene-quartz skarn lenses, which crop out on the floor of the cirque. Another poorly mineralized zone approximately 60 m long and 10 m thick is located in the west wall. Narrow barite veins up to 100 m long can also be found cutting through the hornfels zone developed in Ordovician to Lower Devonian chert and shale units near the contacts of the quartz monzonite stock (Yukon Geological Survey Minfile #105J 015, 1992). The source of the barium sulfate is unknown, but field observations suggest a primary sedimentary origin.

Meierite Mineral Description

Mineral name

The new mineral and name have approved by the Commission on New Minerals, Nomenclature and Classification of the International Mineralogical Association (IMA 2014-039). The type specimen is deposited in the collections of the Royal Ontario Museum and has been assigned specimen number M56744.

Meierite is named after Walter M. Meier (1926–2009) (Fig. 2). Meier & Kokotailo (1965) determined the atomic structure of the synthetic material ZK-5 (KFI type), which exhibits the same framework topology as meierite. Walter M. Meier was one of the driving forces behind the founding of the International Zeolite Association (IZA) and, together with Jan Uytterhoeven, organized the Third International Zeolite Conference (IZC) in 1973 in Zurich, Switzerland. At the following IZC in Chicago, he founded the Structure Commission of the IZA, which he then chaired for the next 12 years. He will probably be best remembered as an author of the first five editions of the Atlas of Zeolite Framework Types (Baerlocher *et al*. 2001). The three-letter codes that we use today as a matter of course stem from that work. His fascination with the synthesis and structural characterization of zeolitic materials started with his dissertation research under Prof. Richard M. Barrer at Imperial College in London in the 1950's (Barrer & Meier 1958), developed further during his long tenure as Professor at the ETH in Zurich, and continued well beyond his official retirement in 1992.

Fig. 2. Walter M. Meier (1926–2009) determined the atomic structure of zeolite ZK-5, which has the same atomic structure as the new mineral species, meierite, described here.

Occurrence and associated minerals

The physical properties observed for meierite are given in Table 1. Meierite occurs as equant grains up to 200 μm across, enclosed within large gillespite crystals (Figs. 3 and 4a). When the meierite is not completely enclosed by gillespite it is observed to alter to a mixture of cerchiaraite-(Fe) and hedenbergite (Fig. 4b). Edingtonite [$Ba(Al_2Si_3O_{10})\cdot 4H_2O$] also occurs as small white equant grains enclosed in gillespite.

Chemical composition

The chemical composition of meierite was determined by electron microprobe analysis of mineral grains in a polished thin section (Fig. 3) using a JEOL JXA-8230 electron microprobe equipped with five wavelength-dispersive spectrometers. The accelerating voltage was 15 kV, and the beam current measured on the Faraday cup was 10 nA. The beam was defocused to produce a ~7 μm spot. No obvious change in the appearance of the mineral was observed in backscattered electron images collected before and after

TABLE 1. PHYSICAL PROPERTIES OF MEIERITE

Color	white/clear
Streak	white
Luster	vitreous, transparent
Fluorescence	none
Hardness	5½ (estimated)
Cleavage	none observed
Tenacity	brittle
Fracture	conchoidal
Density	(calculated) 3.50 g/cm^3
Optical Properties	
(Na vapor light source, 589 nm)	
Isotropic $n = 1.598$	
Compatibility index $(1 - (K_p/K_c)) = 0.029$ (excellent)	

analysis. Peak and background count times for each element were 10 s. Standards were adularia (Si, Al, K), rutile (Ti), barite (Ba), synthetic fayalite (Fe), anorthite glass (Ca), albite (Na), synthetic $Ca_2P_2O_7$ (P), and scapolite (Cl). Ti$K\alpha$ was measured using a LiF diffracting crystal in order to avoid interference from Ba$L\alpha$; Ti was present at a concentration near its detection limit. Data were treated using the XPP matrix correction algorithm of Pouchou & Pichoir (1991), and the results (average of 11 analyses) are presented in Table 2.

Assuming a complete tetrahedral framework of tetrahedrally coordinated Si, Al, and P, and the charges of the other cations, there is a net positive charge of 33.4. If this is balanced by OH^- groups within the open cavities of the structure this would account for an additional 4.29 wt.% and brings the total for the chemical analysis to close to 100%. These OH groups are closely associated with barium and chlorine within the zeolite cavity. The chemical formula determined using this charge balance approach is $Ba_{41.1}Na_{0.7}K_{0.6}Fe_{0.5}Ca_{0.5}Ti_{0.1}[Si_{62.5}Al_{30.5}P_{3.0}]_{96}O_{192}Cl_{24.82}(OH)_{33.4}$ and this can be simplified to $Ba_{44}Si_{66}Al_{30}O_{192}Cl_{25}(OH)_{33}$. Table 2 shows the calculation of charge balance based on the microprobe-measured composition. The open silicate framework with large cavities allows for considerable variation of chemical composition and it is not possible to be more specific with respect to the OH and total H_2O contents. Due to the small amount of material available, no thermogravi-

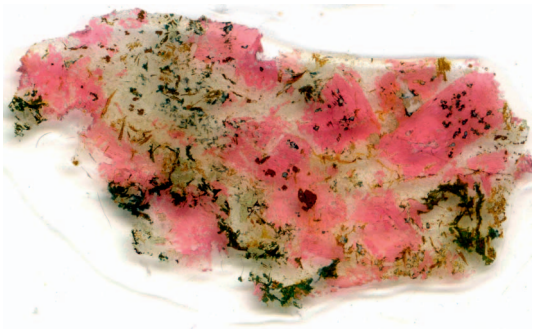

FIG. 3. A thin section showing large gillespite crystals (pink) enclosing meierite, cerchiaraite-(Fe), pellyite, and hedenbergite. Meierite occurs as clear sub-millimeter equant inclusions within the gillespite crystals. Field of view is 40 mm.

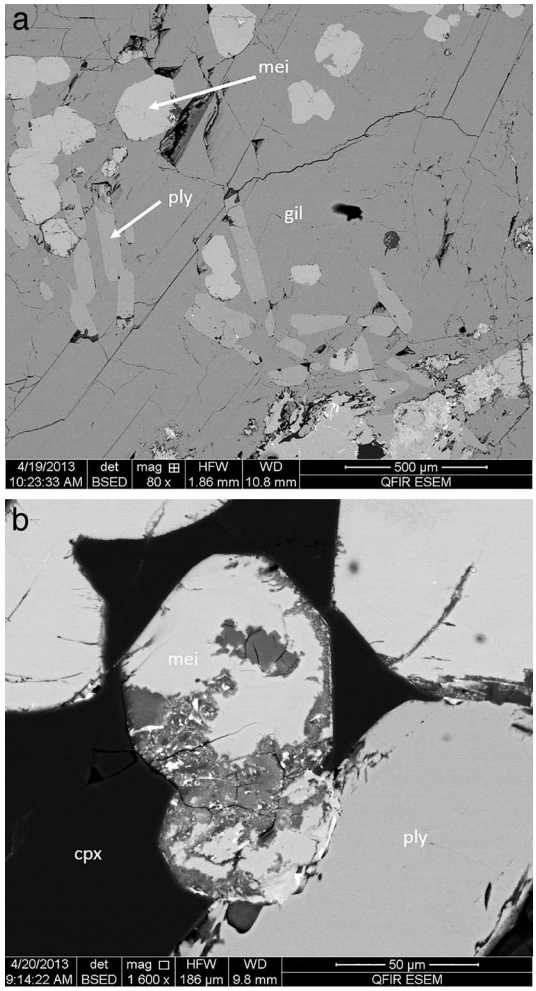

FIG. 4. (a) Backscattered electron image of unaltered equant grains of meierite (mei) enclosed in gillespite (gil) and associated with pellyite (ply). (b) Backscattered electron image of equant grains of meierite adjacent to hedenbergite (cpx) and pellyite (ply). This crystal of meierite is altering to a fine-grained mixture of cerchiaraite-(Fe) and hedenbergite.

TABLE 2. CHEMICAL COMPOSITIONS OF MEIERITE

	wt.% oxide	Molecular weight	# Cations	# Oxygens	# Cations based on 96T	Charge
SiO_2	28.30	60.02	0.47	0.94	62.47	249.86
P_2O_5	1.61	141.95	0.02	0.06	3.00	15.00
Al_2O_3	11.75	101.94	0.23	0.35	30.53	91.60
TiO_2	0.05	79.9	0.00	0.00	0.09	0.34
FeO	0.27	71.85	0.00	0.00	0.49	0.98
CaO	0.21	56.08	0.00	0.00	0.49	0.98
BaO	47.61	153.36	0.31	0.31	41.13	82.25
Na_2O	0.15	61.98	0.00	0.00	0.66	0.66
K_2O	0.21	94.2	0.00	0.00	0.59	0.59
Cl	6.64	35.45	0.19		24.82	–24.82
Total	96.79					
O = Cl	1.50					
Total	95.29				total + charge	442.27
					chg O, Cl	–408.82
OH^-	4.29	17	0.25		excess +ve	33.44
total	99.58					

Note: Formula based on site occupancies from structure refinement: $Ba_{39.9}Ca_{2.01}Si_{96}O_{192}Cl_{28.8}(H_2O,OH)_{44.5}$
Formula based on chemical analysis and charge balance considerations: $Ba_{41.1}Ca_{0.5}Fe_{0.5}Na_{0.7}K_{0.6}Si_{62.5}Al_{30.5}P_{3.0}O_{192}Cl_{24.8}(OH)_{33.4}$

metric analysis was conducted nor were experiments conducted to evaluate the molecular exchange capacity of this mineral.

X-ray powder diffraction

X-ray powder diffraction data were recorded with a PANalytical X'Pert Powder diffractometer [Cu$K\alpha$(Ni) radiation] equipped with an X'Celerator detector. The hand-picked mineral concentrate sample was finely ground and dusted onto a zero-background silicon sample holder. Some gillespite and quartz could not be separated and removed and remained in the sample. Observed *d* spacings and intensities were derived by profile fitting using PANalytical HighScore Plus software (version 4.1) (Table 3).

Atomic structure

The atomic structure of synthetic zeolite $Na_{30}Al_{30}Si_{66}O_{192}\cdot 98H_2O$ was determined by Meier & Kokotailo (1965) in space group $Im\bar{3}m$ using powder diffraction data. This was labelled zeolite ZK-5 and is the KFI structure type listed in the Atlas of Zeolite Structures (Baerlocher *et al*. 2001). Parise *et al*. (1983) determined the atomic structure of the zeolites (Cs,K)-ZK-5 and (Cs,D)-ZK-5.

For this study, single-crystal X-ray diffraction measurements were made in the Department of Chemistry at UBC using a Bruker DUO APEX II diffractometer with TRIUMPH monochromated Mo $K\alpha$ radiation. Data were collected in a series of φ and ω scans in 0.50° oscillations with 20 s exposures. The crystal-to-detector distance was 60 mm. Data were collected and integrated using the Bruker SAINT software package. Data were corrected for absorption effects using the multi-scan technique (SADABS) and were corrected for Lorentz and polarization effects.

All refinements were performed using the SHELXTL crystallographic software package of Bruker AXS. Scattering factors for neutral atoms were used for the cations and ionic factors for O^{2-} were used for oxygen. The weighting scheme was based on counting statistics. Neutral-atom scattering factors were taken from Cromer & Waber (1974). Anomalous dispersion effects were included in F_{calc} (Ibers & Hamilton 1964); the values for $\Delta f'$ and $\Delta f''$ were those of Creagh & McAuley (1992). The values for the mass attenuation coefficients are those of Creagh & Hubbell (1992). The atomic structure of meierite was determined using the atomic coordinates of Meier & Kokotailo (1965) as starting coordinates. Details of the data collection and refinement are given in Table 4. Tables 5, 6, and 7 list the atomic coordinates, atomic displacement parameters, and selected bond lengths. The unit cell dimension of 18.5502(4) is slightly shorter than the range exhibited for other KFI-type materials. This may reflect a limited substitution of P for Si at the tetrahedral sites. The ratio of Si/Al/P is 62.5/30.5/3.0 and the smaller radii of P^{5+} would result in a slight collapse of the tetrahedral framework.

The structure of meierite (KFI) is not only related to framework type RHO but also to LTA. The central cavity that is common to all is an *lta* cavity which

TABLE 3. POWDER DIFFRACTION DATA

I (obs.)	*d* (obs) [Å]	*d* (calc) [Å]	*hkl*
12	9.34	9.29	200
4	5.894	5.875	310
14	4.977	4.965	321
70	4.388	4.379	411, 330
26	4.161	4.154	420
2	4.030	4.054	421
25	3.798	3.792	422
12	3.648	3.643	510, 431
34	3.288	3.284	440
2	3.244	3.234	441, 522
100	3.189	3.186	433, 530
3	3.142	3.140	531
22	3.100	3.096	442, 600
72	3.016	3.014	611, 532
8	2.939	2.937	620
42	2.803	2.801	622
31	2.629	2.627	710, 550, 543
28	2.529	2.528	721, 552, 633
3	2.484	2.483	642
12	2.441	2.439	730
9	2.382	2.379	650, 643
5	2.361	2.359	651, 732
46	2.323	2.322	800
59	2.287	2.287	741, 554, 811
12	2.254	2.253	820, 644
9	2.240	2.237	821, 742
6	2.221	2.221	653
5	2.159	2.160	750, 831, 743
3	2.104	2.104	752
2	2.081	2.077	840
4	2.052	2.052	910, 833
8	2.027	2.027	842
9	2.004	2.003	761, 921, 655
4	1.958	1.958	930, 754, 851
3	1.943	1.948	931

Note: There are two additional peaks in the pattern, the gillespite (002) peak (*I* 10) and the main quartz peak (*I* 7), which were excluded from the fit. The unit cell dimension is 18.578(2) Å based on least-squares refinement of powder diffraction data.

consists of 4-, 6-, and 8-membered rings. In these three structure types the *lta* cavities are connected through different composite building units, either d4r (LTA), d6r (KFI), or d8r (RHO). In doing so, additional cavities are generated: *sod* cavities for LTA and *pau* cavities for KFI. In RHO an additional *lta* cavity is generated. This relationship is illustrated in Meier & Kokotailo (1965). In meierite, the *lta* cavities are connected in the [111] direction through d6r with an approximate free diameter of 3.2 Å (Fig. 5). The large cavities are also connected by the *pau* cavity along the [100] direction with an approximate free diameter of 3.9 Å. In the final cycles of least-squares refinement the barium, chlorine, and hydroxyl site occupancies of the intra-framework sites were assigned so that the chemical composition of the atomic structure model closely matched the composition determined by microprobe analysis.

TABLE 4. SINGLE CRYSTAL X-RAY DIFFRACTION DATA COLLECTION AND ATOMIC STRUCTURE REFINEMENT DETAILS

Space group	$Im\bar{3}m$ (229)
a (Å)	18.5502(4)
V (Å^3)	6383.3(2)
Z	1
Crystal size (mm)	0.23 × 0.18 × 0.17
Radiation	Mo$K\alpha$
Monochromator	TRIUMPH
$2\theta_{max}$ (°)	72.56
h, *k*, *l* ranges	–30/22, –30/18, –30/27
Total reflections	29165
Unique reflections	1531
$F_o > 4\sigma(F_o)$	1393
$R_{int.}$ (%)	3.66
R_σ (%)	2.12
R_1 for $F_o > 4\sigma$ (%)	4.07
R_1 for all unique F_o (%)	4.47
wR_2 (%)	10.76
GooF (=S)	1.130
i	0.0343
j	75.4788
$\Delta\rho_{max}$ (e/Å^3)	2.74
$\Delta\rho_{min}$ (e/Å^3)	–3.68

$R_1 = \sum (F_o - F_c)/ \sum F_o$, $w = 1/(\sigma^2(F_o^2) + (i \times P)^2 + j \times P)$ where $P = [\text{Max.}\ (F_o^2,0) + 2F_c^2]/3$; $wR_2 = [(\sum w(F_o^2 - F_c^2)^2)/\sum w(F_o^2)^2]^{1/2}$

Figure 6 shows the location of the intra-framework atoms for the structure model presented here. The requirement that some sites are partially occupied and disordered is expected in such an open framework cavity. Of five anion sites in the framework cavity, only the split site Cl1/OH5 is fully occupied. The sites Cl2, Cl3, OH6, and OH7 are all partially occupied. In particular, Cl2, OH6, and OH7 are all within 2 Å of each other and other symmetry-equivalent sites, and so cannot be fully occupied.

Four Ba sites are located in the cavities of the KFI framework. The Ba1 site is 12-coordinated by 4 × O1, 4 × O2, and 4 × Cl1/OH5. Each Ba1 polyhedron shares a Cl1/OH5 vertex with three adjacent Ba1 polyhedra, and O1–O2 edges with four Si1 tetrahedra; the Ba1 polyhedra thus form a network that interpenetrates and shares edges with the tetrahedral framework.

TABLE 5. ATOMIC COORDINATES OF MEIERITE

Atom	*x*	*y*	*z*	*U*(iso)	Occupancy
Ba1	1/4	1/2	0	0.02747(15)	1
Ba2	0.36871(3)	0.36871(3)	0.36871(3)	0.0333(2)	0.874(5)
Ca2	0.3533(8)	0.3533(8)	0.3533(8)	0.024(3)	0.126(5)
Ba3	0	0.37395(12)	0.0149(2)	0.0675(12)	0.2604(16)
Ba4	0	0	0	0.0575(12)	0.705(11)
Si1	0.30008(4)	0.41779(4)	0.18076(4)	0.01292(14)	1
Cl1	0.09523(10)	0.5	0.09523(10)	0.0393(8)	0.89(2)
Cl2	0	0.1720(5)	0	0.034(3)	0.285(16)
Cl3	0.25	0.25	0.25	0.019(7)*	0.076(13)
O1	0.25	0.38273(16)	0.11727(16)	0.0298(7)	1
O2	0.1828(2)	0.34807(18)	0	0.0266(7)	1
O3	0.26087(13)	0.26087(13)	0.41622(17)	0.0247(6)	1
O4	0.37780(15)	0.37780(15)	0.1922(2)	0.0287(7)	1
OH5	0.09523(10)	0.5	0.09523(10)	0.0393(8)	0.11(2)
OH6	0.0427(15)	0.2210(15)	0	0.19(2)*	0.50(2)
OH7	0	0.1323(10)	0.0695(10)	0.082(6)*	0.428(16)

Note: * indicates *U*(eq)

TABLE 6. ATOMIC DISPLACEMENT PARAMETERS FOR MEIERITE (Å^2)

	U_{11}	U_{22}	U_{33}	U_{12}	U_{13}	U_{23}
Ba1	0.0403(3)	0.02105(16)	0.02105(16)	0	0	0
Ba2	0.0333(2)	0.0333(2)	0.0333(2)	–0.00522(16)	–0.00522(16)	–0.00522(16)
Ca2	0.024(3)	0.024(3)	0.024(3)	0.003(3)	0.003(3)	0.003(3)
Ba3	0.070(3)	0.0952(12)	0.0369(12)	–0.0132(8)	0	0
Ba4	0.0575(12)	0.0575(12)	0.0575(12)	0	0	0
Si1	0.0132(3)	0.0096(3)	0.0159(3)	–0.0009(2)	–0.0007(2)	0.00055(19)
Cl1	0.0407(9)	0.0365(11)	0.0407(9)	0	0.0106(8)	0
Cl2	0.035(3)	0.031(5)	0.035(3)	0	0	0
O1	0.0219(14)	0.0338(11)	0.0338(11)	–0.0119(14)	–0.0050(8)	–0.0050(8)
O2	0.0452(19)	0.0232(14)	0.0114(11)	0	0	0.0095(13)
O3	0.0244(9)	0.0244(9)	0.0253(14)	–0.0012(8)	–0.0012(8)	0.0045(11)
O4	0.0242(9)	0.0242(9)	0.0378(19)	–0.0065(10)	–0.0065(10)	0.0097(12)
OH5	0.0407(9)	0.0365(11)	0.0407(9)	0	0.0106(8)	0

TABLE 7. SELECTED BOND LENGTHS IN MEIERITE (Å)

Bond	Distance	Bond	Distance
Ba1–O1	3.076 (4) ×4	Ba3–O2	3.151 (5)
Ba1–O2	3.082(4) ×4	Ba3–O4	3.257 (5) ×2
Ba1–Cl1/OH5	3.3710(6) ×4	Ba3–Cl1	3.288 (3) ×2, 3.572(3) ×2
Ba2–O3	2.963(4) ×3	Ba3–OH5	3.288
Ba2–O4	3.283(4) ×3	Ba3–OH6	2.88(3), 2.96(3) ×2, 3.03(3)
Ba2–OH7	2.692(8) ×6	Ba4–OH7	2.77(2) ×24
Ba2–Cl2	3.562(2) ×3	Ba4–Cl2	3.19(1) ×6
Ca2–O3	2.69(1) ×3		
Ca2–O4	3.06(1) ×3		
Ca2–OH7	3.09(2) ×6		
Ca2–Cl3	3.32(2)		

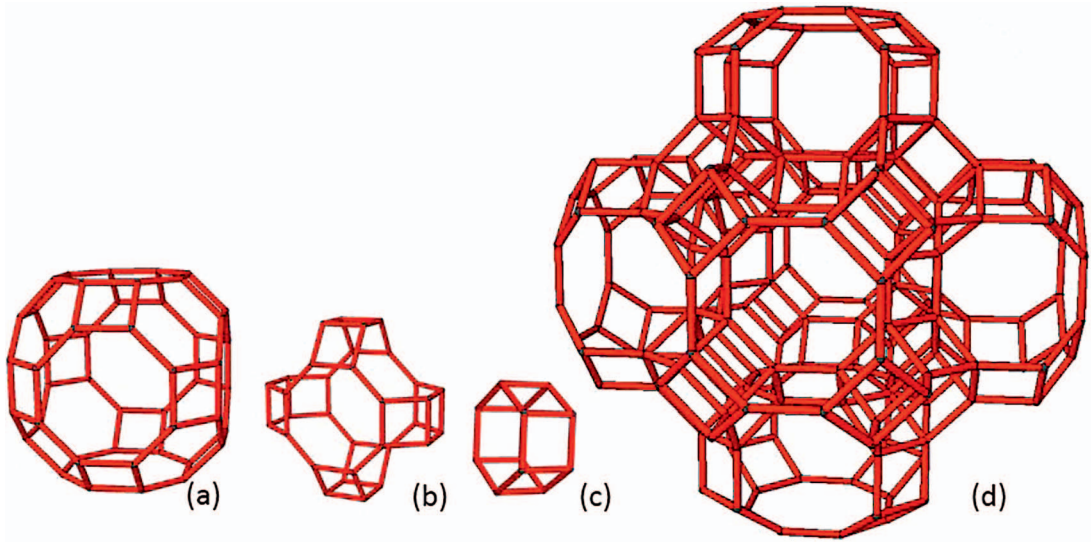

FIG. 5. The linkage of the tetrahedral framework in meierite. Lines connect the centers of framework tetrahedra. (a) The *lta* cubo-octahedral cavity. (b) *pau* cavity. (c) 6dr cavity. (d) Connectivity of these cavities using *pau* cavity along the **a** axis and the d6r cavity along [111].

The Ba2 sites lie on the [111] directions just above and below double six-membered rings of tetrahedra. Each Ba2 is coordinated by 3 × O3 and 3 × O4 from the adjacent six-membered ring, and formally by 6 × OH7 and 3 × Cl2, not all of which can be occupied simultaneously. During refinement a second center of electron density adjacent to Ba2 was found and labelled Ca2, with the total occupancy Ba2 + Ca2 constrained to be equal to 1. Eight adjacent Ba2/Ca2 polyhedra form a cavity around the Ba4 site. Ba4 is formally coordinated by 24 × OH7 and 6 × Cl2, but due to partial occupancy of these anion sites its true average coordination is likely around 10–12.

The Ba3 site lies in a double eight-fold ring cavity (Fig. 6c), slightly displaced from a four-fold rotational symmetry axis, leading to an occupancy of ~1/4. Ba3 is formally coordinated by 1 × O2, 2 × O4, 4 × Cl1/OH5, 1 × Cl2, and 6 × OH6; due to partial occupancy of Cl2 and OH6, its true average coordination is again likely to be 10–12. The Ba3 polyhedra form face-sharing dimers, with a Ba3–Ba3 distance across the 4 × Cl1/OH5 face of 4.693(5) Å.

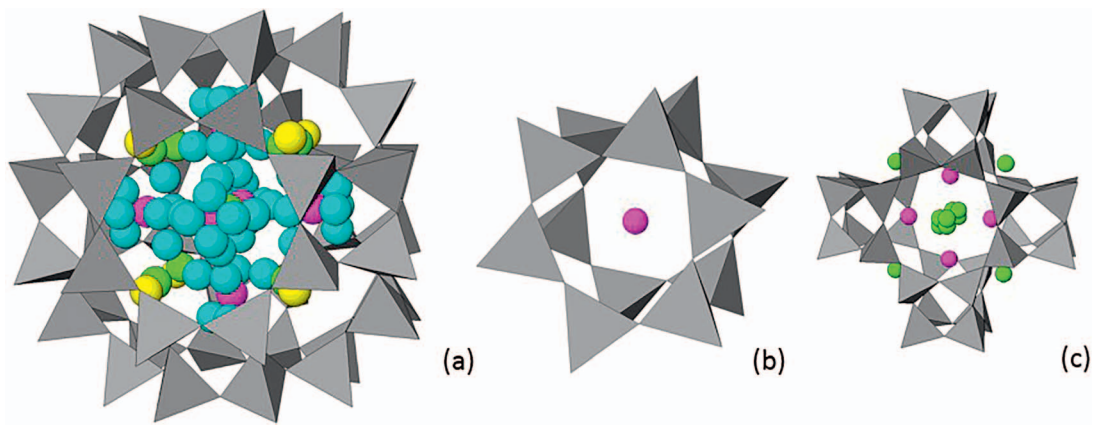

FIG. 6. Ba (green and yellow), Cl (pink), and OH (blue) locations within (a) the central cubo-octahedral cavity (*lta*), (b) the double six-fold ring cavity (d6r), and (c) the *pau* cavity (d8r).

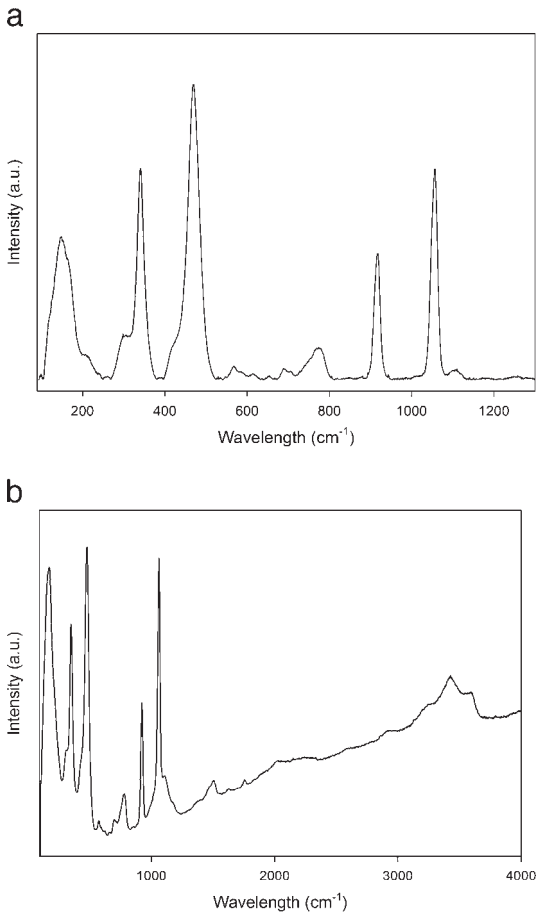

FIG. 7. Raman spectra of meierite showing the main Raman bands in the region 100–1400 cm^{-1} (top). The spectrum below shows the O–H stretching vibrations bands located between 3100 and 3680 cm^{-1}.

Raman spectroscopy

The Raman spectrum of meierite was collected from a randomly oriented crystal using a Thermo-Almega microRaman system, with a 532 nm solid-state laser and a thermoelectric cooled CCD detector. The laser is partially polarized with 4 cm^{-1} resolution and a spot size of 1 μm. The Raman spectrum of meierite is shown in Figure 7. Based on previous Raman spectroscopic studies of various zeolites (Dutta & Zaykoski 1988, Smirnov *et al*. 1994, Knops-Gerris *et al*. 1997, Goryainov & Smirnov 2001, Yu *et al*. 2001, Liu *et al*. 2012, Yang *et al*. 2013), we made a tentative assignment of major Raman bands for meierite. The O–H stretching vibrations bands are located between 3100 and 3680 cm^{-1}. The bands between 880–1130 cm^{-1} and those between 670 and 830 cm^{-1} correspond to the T–O anti-symmetric and symmetric stretching vibrations (ν3 and ν1 modes) within the TO_4 groups, respectively (T = Al, Si). The bands between 260 and 560 cm^{-1} are ascribed to the T–O–T bending vibrations. Below 200 cm^{-1}, the bands are related to the rotational and translational modes of TO_4 tetrahedra, as well as lattice vibrational modes. Similar to other zeolite-type structures (*e.g*., Yang *et al*. 2013), in meierite the Raman bands associated with the T–O symmetric stretching vibrations are less intense than those corresponding to the T–O asymmetric stretching modes due to the complex vibrations of the TO_4 tetrahedra coupled through sharing of the O at the corners (Wopenka *et al*. 1998). In contrast, isolated TO_4 tetrahedra usually have symmetric stretching vibrations more intense than the asymmetric stretching modes.

DISCUSSION

Barrer & Robinson (1972) determined the atomic structures of two salt-bearing aluminosilicates, called species P (grown from a gel using $BaCl_2$) and Q (grown from a gel using $BaBr_2$) (both are isotypic with KFI). Species P had the cell content $Ba_{15}[Al_{30}Si_{66}O_{192}]$ $1.7Ba(OH)_2$, $12.5BaCl_2$, $35H_2O$. The details of the synthesis of species P and Q from gels is described by Barrer & Marcilly (1970); they demonstrated that the $BaCl_2$ could be hydrothermally extracted from phase P using distilled water and that the resulting material had "the same sieve properties as chabazite or Linde Sieve 5A". Synthesis of KFI structure zeolites may also be accomplished by growing the zeolite in a media with large organic molecules that serve to hold the tetrahedral framework open as crystallization takes place. A KFI-type zeolite has been grown by using 18-crown-6 ether as an organic template from a starting aluminosilicate gel containing potassium and strontium ions (Chatelain *et al*. 1996). Once the KFI structure is stable, the organic molecules can be removed by calcination.

The natural occurrence of meierite is due to the unusual natural abundance of Ba and Cl combined with OH^- during crystal growth in the low-temperature aqueous environment of this skarn deposit. These large atoms hold the silicate tetrahedral framework open as the three-dimensional framework crystallizes. The exchange behavior of meierite could not be demonstrated because of the limited amount of material. However, the close similarity in composition and structure type of meierite to the type P material grown by Barrer & Marcilly (1970), where sieve properties have been demonstrated, suggests that the Ba and Cl in meierite is also exchangeable under hydrothermal conditions. This exchange ca-

pacity may also explain why meierite crystals that are completely enclosed in gillespite have not been altered, but those that are not enclosed have been altered subsequent to formation.

Acknowledgments

Christian Baerlocher is thanked for drawing the author's attention to the work of Barrer and Robinson. The manuscript was significantly improved by reviews by Dr. Christian Lengauer and an anonymous reviewer. Henrik Friis is thanked for editorial assistance. The authors also wish to thank Warren LeFave and the staff of the Inconnu Lodge for support during the field work. NSERC Discovery Grants to RCP and LAG supported the research.

References

Alfors, J.T. & Pabst, A. (1984) Titanian taramellites in western North America. *American Mineralogist* **69**, 358–373.

Alfors, J.T., Stinson, M.C., & Matthews, R.A. (1965) Seven new barium minerals from eastern Fresno County, California. *American Mineralogist* **50**, 314–340.

Baerlocher, C., Meier, W.M., & Olson, D.H. (2001) *Atlas of Zeolite Framework types*, *5th Edition*. Published on behalf of the Structure Commission of the International Zeolite Association by Elsevier, New York, Oxford, London (308 pp.).

Barrer, R.M. & Marcilly, C. (1970) Hydrothermal chemistry of silicates. Part XV. Synthesis and nature of some salt-bearing aluminosilicates. *Journal of the Chemical Society A: Inorganic, Physical, Theoretical*, 2735–2745.

Barrer, R.M. & Meier, W.M. (1958) Structural and ion sieve properties of a synthetic crystalline exchanger. *Transactions of the Faraday Society* **58**, 1074–1085.

Barrer, R.M. & Robinson, D.J. (1972) The structures of the salt-bearing aluminosilicates species P and Q. *Zeitschrift für Kristallographie* **135**, 374–390.

Chatelain, T., Patarin, J., Farre, R., Petigny, O., & Schulz, P. (1996) Synthesis and characterization of 18-crown-6 ether-containing KFI-type zeolite. *Zeolites* **17**, 328–333.

Creagh, D.C. & Hubbell, J.H. (1992) *International Tables for Crystallography, Vol C*. Kluwer Academic Publishers, Boston, Massachusetts (200–206).

Creagh, D.C. & McAuley, W.J. (1992) *International Tables for Crystallography, Vol C*. Kluwer Academic Publishers, Boston, Massachusetts (219–222).

Cromer, D.T. & Waber, J.T. (1974) *International Tables for X-ray Crystallography, Vol. IV*. The Kynoch Press, Birmingham, England.

Dutta, P.K. & Zaykoski, R.E. (1988) Raman spectroscopy of metal complexes in zeolite cavities: Cause and removal of interfering photoemission. *Zeolites* **8**, 179–182.

Goryainov, S.V. & Smirnov, M.B. (2001) Raman spectra and lattice-dynamical calculations of natrolite. *European Journal of Mineralogy* **13**, 507–519.

Ibers, J.A. & Hamilton, W.C. (1964) Dispersion corrections and crystal structure refinements. *Acta Crystallographica* **17**, 781–782.

Kampf, A.R., Roberts, A.C., Venance, K.E., Carbone, C., Dunning, G.E., & Walstrom, R.E. (2013) Cerchiaraite-(Fe)and cerchiaraite-(Al), two new barium cyclosilicate chlorides from Italy and California, USA. *Mineralogical Magazine* **77**, 69–80.

Kampf, A.R., Peterson, R.C., & Joy, B.R. (2014) Itsiite $Ba_2Ca(BSi_2O7)_2$, a new mineral species from Yukon, Canada: Description and crystal structure. *Canadian Mineralogist* **52**, 401–407.

Knops-Gerris, P., DeVos, D., Feijen, E., & Jacobs, P. (1997) Raman spectroscopy on zeolites. *Microporous Materials* **8**, 3–17.

Liu, D., Liu, Z., Lee, Y., Seoung, D., & Lee, Y. (2012) Spectroscopy characterization of alkali-metal exchanged natrolites. *American Mineralogist* **97**, 419–424.

Meier, W.M. & Kokotailo, G.T. (1965) The crystal structure of zeolite ZK-5. *Zeitschrift für Kristallographie* **121**, 211–219.

Montgomery, J.H. (1960) *A study of barium minerals from the Yukon Territory*. M.Sc. University of British Columbia, Vancouver, Canada.

Montgomery, J.H., Thompson, R.M., & Meagher, E.P. (1972) Pellyite; a new barium silicate mineral from the Yukon Territory. *Canadian Mineralogist* **11(2)**, 444–447.

Newberry, N.G., Essene, E.J., & Peacor, D.R. (1981) Alforsite, a new member of the apatite group: the barium analogue of chlorapatite. *American Mineralogist* **66**, 1050–1053.

Parise, J.B., Shannon, R.D., Prince, E., & Cox, D.E. (1983) The crystal structures of synthetic zeolites (Cs,K)-ZK-5 and (Cs,D)-ZK-5 determined from neutron diffraction data. *Zeitschrift für Kristallographie* **165**, 175–190.

Pouchou, J.-L. & Pichoir, F. (1991) Quantitative analysis of homogeneous or stratified microvolumes applying the model "PAP". *In* Electron Probe Quantitation (K.F.J. Heinrich & D.E. Newbury, eds.). Plenum Publishing Corporation, New York, New York, United States (31–75).

Smirnov, K., Le Maire, M., Bremard, C., & Bougeard, D. (1994) Vibrational spectra of catio-exchanged zeolite A. Experimental and molecular dynamics study. *Chemical Physics* **179**, 445–454.

Walstrom, R.E. & Leising, J.F. (2005) Barium minerals of the sanbornite deposits, Fresno County, California. *Axis* **1(8)**, 1–18.

Wopenka, B., Freeman, J., & Nikischer, T. (1998) Raman spectroscopic identification of fibrous natural zeolites. *Applied Spectroscopy* **52**, 54–63.

Yang, H., Downs, R.T., Evans, S.H., Jenkins, R.A., & Bloch, E.M. (2013) Rongibbsite, $Pb_2(Si_4Al)O_{11}(OH)$, a new zeolitic aluminosilicate mineral with an interrupted framework from Maricopa County, Arizona, U.S.A. *American Mineralogist* **98**, 236–241.

Yu, Y., Xiong, G., Li, C., & Xiao, F. (2001) Characterization of aluminosilicate zeolites by UV Raman spectroscopy. *Microporous and Mesoporous Materials* **46**, 23–34.

Received December 11, 2014. Revised manuscript accepted February 22, 2016.